Simulating observed boundary layer clouds on Mars

F. Daerden,[1] J. A. Whiteway,[2] R. Davy,[2] C. Verhoeven,[1,3] L. Komguem,[2] C. Dickinson,[2] P. A. Taylor,[2] and N. Larsen[4]

[1]   A microphysical model for Mars dust and ice clouds has been applied in combination with a model of the planetary boundary layer (PBL) for the interpretation of measurements by the LIDAR instrument on the Phoenix Mars mission. The model simulates nighttime clouds and fall streaks within the PBL that are similar in structure to the LIDAR observations. The observed regular daily pattern of water ice cloud formation and precipitation at the top of the PBL is interpreted as a diurnal process in the local water cycle in which precipitation of large ice crystals ($30-50$ μm effective radius) results in downward transport of water vapor within the PBL. This is followed by strong vertical mixing during daytime, and this cycle is repeated every sol to confine water vapor within the PBL. **Citation:** Daerden, F., J. A. Whiteway, R. Davy, C. Verhoeven, L. Komguem, C. Dickinson, P. A. Taylor, and N. Larsen (2010), Simulating observed boundary layer clouds on Mars, *Geophys. Res. Lett.*, *37*, L04203, doi:10.1029/2009GL041523.

1.   Introduction

[2]   The LIDAR instrument on the Phoenix mission has provided observations of water ice clouds that form and precipitate within the nighttime residual Planetary Boundary Layer (PBL) on Mars [*Whiteway et al.*, 2008, 2009]. It was found that there is a regular diurnal pattern in which water vapor is mixed throughout the PBL by turbulence and convection during daytime and then at night water ice crystals precipitate toward the ground. This process acts to confine water within the PBL and it will enhance the contribution of the local exchange of water between the ground and atmosphere in the hydrological cycle. Such a component of the Mars water cycle was originally anticipated at higher altitudes after the Viking missions [*Kahn*, 1990] but there has been no reported observational evidence prior to the Phoenix Mars mission.

[3]   The Phoenix LIDAR was unique in its ability to resolve internal cloud structure and precipitation fall streaks (Figure 1). The length of the fall streaks indicated that the ice crystals had fall speeds that are consistent with prolate ellipsoids with volume-equivalent radii of 35 μm [*Whiteway et al.*, 2009]. The crystals would then be similar to what is found in cirrus clouds on Earth in the same temperature range, for example hexagonal columns of length 150 microns

and width 50 microns [*Whiteway et al.*, 2004; *Gallagher et al.*, 2005].

[4]   Several studies have carried out detailed microphysical modeling of water ice cloud formation in the atmosphere of Mars in 1D models [e.g., *Michelangeli et al.*, 1993; *Colaprete et al.*, 1999; *Montmessin et al.*, 2002; *Pathak et al.*, 2008]. More simplified cloud schemes have been integrated into Mars GCMs [e.g., *Richardson et al.*, 2002; *Montmessin et al.*, 2004]. The formation of clouds at the top of the PBL as observed by the Phoenix LIDAR has not been reported in previous modeling studies. One reason is that the previous models did not have a sufficiently high vertical resolution within the PBL for an accurate representation of turbulent mixing and radiative transfer. Another problem is the lack of observations to provide a constraint on the vertical profile of humidity.

[5]   These challenges have been addressed in this study by applying a PBL model with high vertical resolution to provide temperature profiles [*Davy et al.*, 2009], and making use of the Phoenix LIDAR and Thermal and Electrical Conductivity Probe (TECP) [*Zent et al.*, 2010] measurements to estimate the profile of humidity [*Whiteway et al.*, 2009]. With this input the detailed microphysical ice cloud model produced a simulation of clouds and precipitation in the PBL that is in agreement with the observations.

2.   Model Setup

[6]   A validated microphysical model for polar stratospheric and cirrus clouds on Earth [*Larsen*, 2000; *Larsen et al.*, 2002, 2004; *Daerden et al.*, 2007] has been modified to Martian conditions. The computational core of the model is kept, while the relevant atmospheric parameters have been replaced by their values for Mars. The model describes nucleation of water ice on dust particles, condensation and evaporation of water vapor onto and from ice particles, sedimentation and eddy diffusion. Solid dust and water ice particles are described by size-binned distributions of their number densities and ice water content. In the present study 100 size bins are used, geometrically increasing from 10 nm to 1 mm. The dust particles are assumed spherical and have a homogeneous mass density of 2.5×10^3 kg/m^3 [*Murphy et al.*, 1990]. The ice particles have an aspect ratio of 3, comparable to the columnar shapes found in terrestrial cirrus clouds [*Whiteway et al.*, 2004; *Gallagher et al.*, 2005]. In the case of low Reynolds numbers, ice particles are assumed to be prolate ellipsoids, for which the terminal fall velocity can be calculated exactly [*Fuchs*, 1964]. In conditions where the Reynolds number exceeds the threshold of 10^{-2}, the empirical expression of *Beard* [1976] is applied for the terminal fall velocity. The size variable is the "volume-equivalent radius", i.e. the radius of a sphere with the same volume as the actual particle.

[1]Belgian Institute for Space Aeronomy, Brussels, Belgium.
[2]Department of Earth and Space Science and Engineering, York University, Toronto, Ontario, Canada.
[3]Now at Department of Mathematics, Free University of Brussels, Brussels, Belgium.
[4]Danish Meteorological Institute, Copenhagen, Denmark.
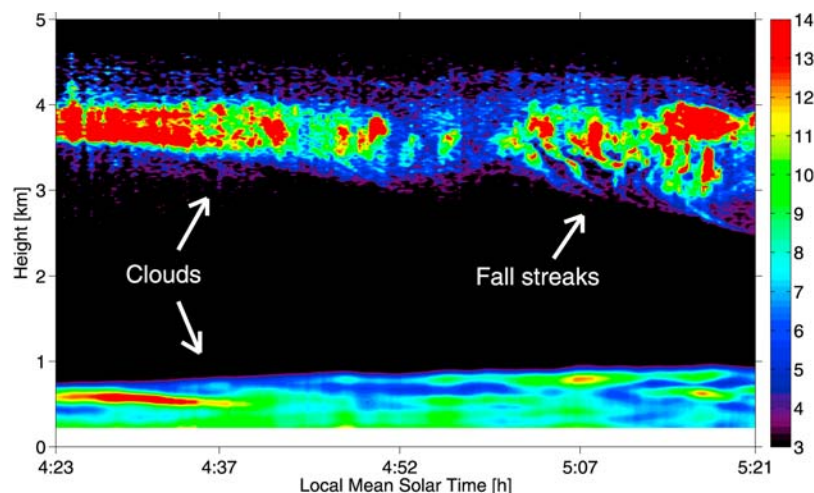
Figure 1. Contour plot of backscatter coefficient derived from the LIDAR backscatter signal at wavelength 532 nm on Phoenix sol 99 (Ls = 122°).

[7] The microphysical model is driven by the temperatures and vertical eddy diffusion coefficients calculated independently by the coupled PBL-Aeolian dust model of *Davy et al.* [2009] for //the Phoenix lander site (lat = 68.2°, lon = 234.2°) at solar longitude// Ls = 122° (Phoenix mission sol 99), see Figure 2a. For the simulations used here the PBL model was constrained to match the Phoenix air temperature measurements at a height of 2 meters above the surface [*Davy et al.*, 2010], and the upper level wind was prescribed as 5 m/s. The model predicts a PBL depth of 4 km, which is consistent with the LIDAR daytime dust observations. The microphysical model is run on the same grid and domain as the PBL model, 241 levels over 30 km with a log-linear grid for good near-surface resolution (41 levels from surface to PBL top). The temperatures are provided to the microphysical simulations at an hourly resolution and are interpolated by a cubic spline to the external time step of the microphysical model, which is 1 Mars-minute. After the PBL model has been running for 15 sols the microphysical model starts at 4 p.m. Mars local solar time. The initial size distribution of dust in the microphysical model is a gamma distribution with r_{eff} = 1.6 μm and ν_{eff} = 0.2 [*Tomasko et al.*, 1999] as in the PBL model. The dust is distributed evenly within the PBL as indicated by the LIDAR observations. The total dust number density is set to approximately 3 particles/cm^3, which corresponds to a backscatter coefficient of ~1.3 × 10^{-6} m^{-1}sr^{-1}, consistent with the LIDAR measurements.

[8] *Whiteway et al.* [2009] estimated the volume mixing ratio of water vapor throughout the residual boundary layer prior to cloud formation at a value of 0.0014 uniformly distributed with height. A value of 0.0013 was used in these simulations. Near the surface the TECP instrument on Phoenix measured a diurnal cycle in water vapor ranging from 2 Pa during the day to less than 0.1 Pa in the early morning, or 0.0027 to 0.00013 in volume mixing ratio [*Zent et al.*, 2010]. Prior to cloud formation, a transition zone of depth 1 km above the surface was assumed in which the water vapor volume mixing ratio decreases linearly with altitude from 0.0027 to the uniformly mixed part of the PBL (see Figure 4d). The resulting water column amount in the PBL is 38 pr-μm.

[9] Ice crystals are formed by nucleation and subsequent vapor deposition onto the dust particle cores. Only heterogeneous nucleation by surface diffusion is considered [*Määttänen et al.*, 2005; *Vehkamäki et al.*, 2007]. Simulations with a contact parameter of m=0.98 resulted in the best agreement with the LIDAR observations. The critical supersaturation ratio for nucleation to start off in the model was a posteriori found to be 10% for results that best match the LIDAR measurements. The fraction of nucleated particles is typically a few percent. After nucleation, ice particles grow and shrink through deposition and sublimation following the basic vapor diffusion equation [*Pruppacher and Klett*, 1997], applying a full kinetic approach [*Toon et al.*, 1989] and taking into account the Kelvin effect, exchange of latent heat, ventilation effects for diffusion and heat transfer, and effects from the nonsphericity of the particles. There is no radiative feedback from the microphysics to the PBL model.

[10] For direct comparison with the LIDAR measurements the optical properties of the modeled dust and ice are calculated in the model at 532 nm. The backscatter coefficient and optical extinction are calculated using the extended-precision T-matrix method for randomly oriented nonspherical particles [*Mishchenko and Travis*, 1998]. The refractive index for dust is 1.518 + 0.0068 i [*Ockert-Bell et al.*, 1997] and for ice 1.31 + 10^{-8} i. The T-matrix calculations did not converge well for larger particles (~10 μm), which is a reported problem for particles of large aspect ratios [*Mishchenko and Travis* 1998]. At present a maximal aspect ratio of 2 is applied in the optical calculations for ice, and for particles larger than the convergence radius a simple extrapolation is applied based on the empirical finding that the scattering efficiency is nearly constant for large particles.

3. Cloud Simulations

[11] The model simulation produced a cloud layer near the surface and a cloud near the PBL top (Figure 2b). The surface cloud formed at 10 p.m. and lasted until 6 a.m. At 5 a.m. it reached a maximal height of 900 m, consistent with the LIDAR observations (Figure 1). The PBL top cloud formed at 1 a.m., lasted through the early morning, and
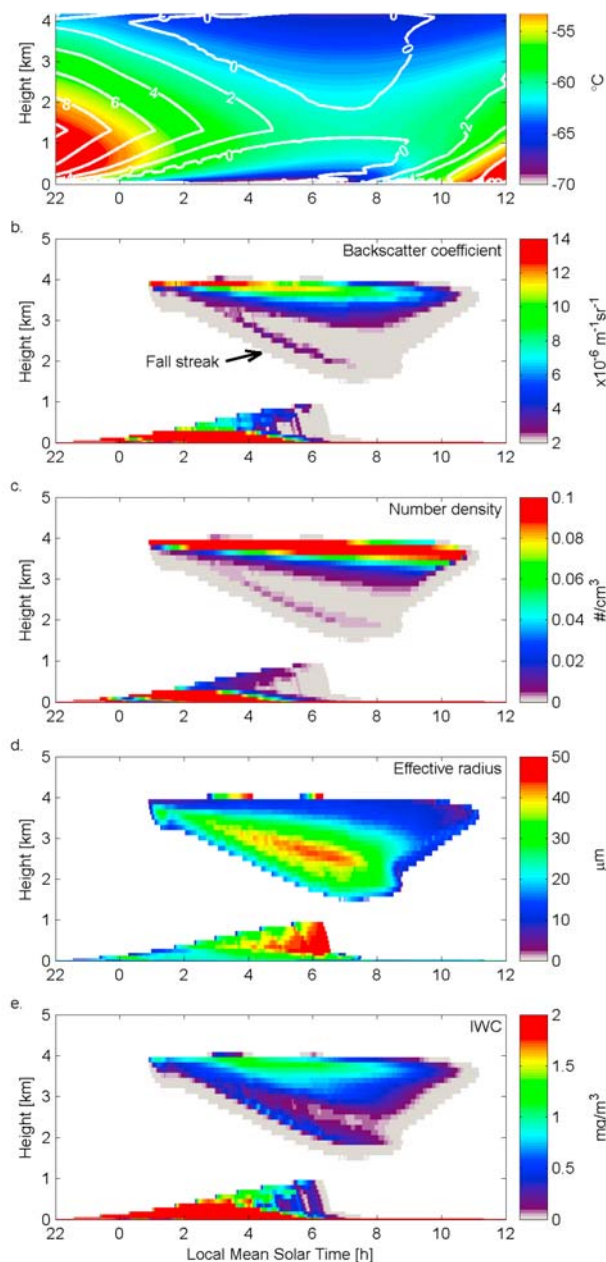
Figure 2. (a) Temperatures interpolated from hourly PBL model output. Contour lines indicate elevation above frost point temperature. Model calculations: (b) backscatter coefficient at 532 nm; (c) ice particle number density; (d) ice particle effective volume-equivalent radius, the length of an ice ellipsoid is ∼4.16 × this value; and (e) cloud ice water content.

dissipated before local noon. The bulk of the cloud was located between 3.5 and 4 km, also consistent with the LIDAR observations. From the top cloud a layer of enhanced number density and backscatter coefficient is descending, which we can characterize as a fall streak. This fall streak formed at 1 a.m. and reached down to height 2.5 km at 5 a.m. which is similar to the observed fall streaks.

[12] Correspondence with the LIDAR measurements on sol 99 was improved by introducing a small and short temperature fluctuation (amplitude < 0.5 K) at the PBL top at

the cloud formation time. This increased the instantaneous cooling rate which affects the ice crystal size and the amount of precipitation. In this case, the small fluctuation led to the formation of more smaller ice particles, strengthening the bulk of the cloud at the PBL top. The fluctuation is not needed to produce a cloud but without it the fall streak would be more pronounced. We expect that there would be similar temperature fluctuations due to gravity waves, shear instability (Kelvin-Helmholtz waves), and overshooting convection.

[13] Figures 2c, 2d and 2e respectively show the modeled ice particle number density, ice particle effective radius, and the ice water content (IWC). Figure 3 gives a more detailed view of the modeled ice particle size distribution at 5 a.m., the time of the LIDAR measurement. Effective radii in the PBL top cloud range from 10 to 20 μm, corresponding to ellipsoids of lengths of 40 to 80 μm. Ice crystals in the fall streak have sizes of 35 ± 5 μm in effective radius and ∼150 μm in length, consistent with the estimate of *Whiteway et al.* [2009]. Such ice crystal sizes had not previously been observed or predicted on Mars, but are typical for ice crystals sampled in cirrus clouds in the upper troposphere on Earth, where the temperatures and humidity are similar to the conditions in the PBL of Mars [*Whiteway et al.*, 2004; *Gallagher et al.*, 2005]. Number densities in the precipitation are ∼0.01 particles per cubic centimeter (Figure 2c). The cloud IWC was calculated by integrating the ice particle size spectrum (Figure 2e). Ice number densities, particle sizes and IWC in the surface layer cloud are typically larger than in the PBL top cloud. The maximal amount of condensed water above 200 m is 2 pr-μm, this corresponds to the estimate of *Whiteway et al.* [2009]. The microphysical model predicts an additional 4 pr-μm of water ice below 200 m of which the largest part is deposited as frost on the surface.

[14] Figure 4a shows the average height profile of the backscatter coefficient at 5 a.m. as derived from the LIDAR measurements, and the comparison with the average model backscatter coefficient. The vertical distribution of the surface and PBL top clouds are in agreement with the observations. Figure 4b shows the derived average optical extinction [*Whiteway et al.*, 2009] and the corresponding model extinction. The optical thickness of both the PBL top cloud and the surface cloud is about 0.1 each.

[15] *Whiteway et al.* [2009] applied two different formulas to derive the cloud IWC from the optical extinction derived
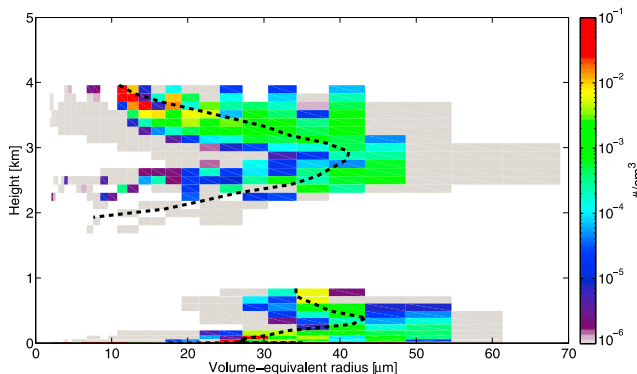
Figure 3. Ice particle size distribution as function of altitude at 5 a.m. The dashed line marks the effective radius.
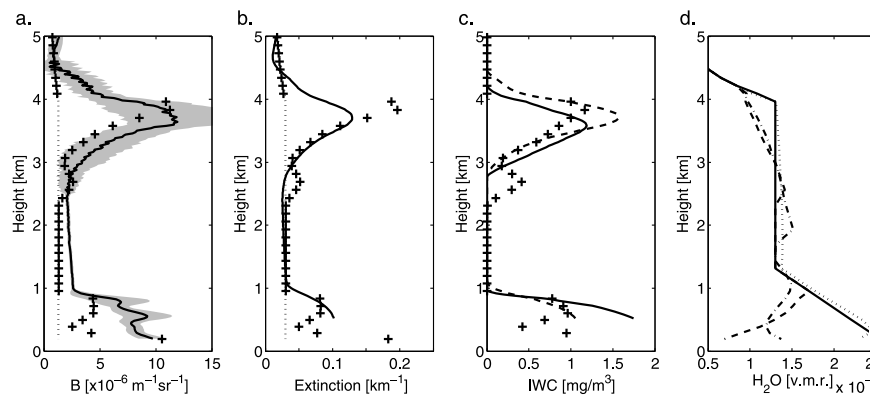
Figure 4. (a) Lidar backscatter coefficient averaged over one hour and smoothed for a vertical resolution of 40 m (full) and the average model backscatter coefficient (crosses). The shaded area is the variability of the measurements (1 standard deviation). The dotted line represents the initial model dust profile. (b) Average extinction profile derived from the LIDAR signal (full) compared to the average model extinction coefficient (crosses). (c) Ice water content derived from the observed LIDAR signal (see text) using the geometrical formula (full line) and the empirical relationship (dashed) compared to the model IWC (crosses). (d) Model water vapor profiles at: initialization (4 p.m., full), 5 a.m. (dashed), 10 a.m. (dash-dotted) and 4 p.m. on the next sol (dotted).

from the LIDAR signal. (1) The geometrical formula where IWC = 4 σ R_{eff} ρ_{ice} / 3 Q with σ the extinction coefficient, R_{eff} the effective radius, ρ_{ice} the water ice density, and Q the scattering efficiency which is assumed 2; and (2) the empirical relationship IWC = 0.119 $\times$ $\sigma^{1.22}$ from cirrus cloud measurements [*Heymsfield et al.*, 2005]. Figure 4c shows that the modeled IWC is in reasonable agreement with both estimates.

[16] The IWC in the modeled fall streak is quite large with 0.5–0.7 mg/m^3. As a result, the precipitation has a considerable impact on the vertical redistribution of water vapor. Figure 4d shows the water vapor profiles at selected times: initial (4 p.m.), at the time of the LIDAR observation (5 a.m.), just after cloud dissipation (10 a.m.), and again at 4 p.m. At the PBL top the water volume mixing ratio decreased by more than 30% to 0.0009, and at the height of 2 km (end of the fall streak) it increased by 15% to 0.0015. Above 3 km there is a net removal of water vapor and below this altitude there is a net increase. In the surface layer cloud the impact on the water vapor is much higher. Close to the surface the water vapor in the model remains saturated over ice throughout the night and reaches a minimum value of ~0.05 Pa between 1 and 4 am. This is in agreement with the measurements by TECP on Phoenix [*Zent et al.*, 2010]. As the sun rises, the surface and atmosphere warm, the ice crystals sublimate, the profile of humidity is mixed again over the PBL during the daytime by turbulence and convection, and the water vapor profile returns to its original shape.

4. Conclusion

[17] It has been demonstrated that the observations by the LIDAR on Phoenix of water ice clouds and precipitation within the PBL on Mars can be reproduced by a numerical simulation that combines models of ice microphysics, boundary layer mixing, and radiative transfer. The main departure of this work from previous modeling studies is that the cloud ice crystals are large enough (30–50 μm

effective radius) that precipitation toward the surface is significant.

[18] In this study the observed clouds at the PBL top are interpreted as indicative of the following diurnal water cycle in the PBL: (1) daytime mixing by convection and turbulence distributes water vapor throughout the PBL; (2) the diurnal temperature variation causes clouds to form at night; (3) large ice crystals fall to lower altitudes within hours; (4) the cloud ice crystals sublimate as the atmosphere warms in the late morning, resulting in a net downward transport of water. The cycle then repeats and water vapor is confined within the PBL.

References

Beard, K. V. (1976), Terminal velocity and shape of cloud and precipitation drops aloft, *J. Atmos. Sci.*, *33*, 851–864, doi:10.1175/1520-0469(1976)033<0851:TVASOC>2.0.CO;2.
Colaprete, A., O. B. Toon, and J. A. Magalhães (1999), Cloud formation under Mars Pathfinder conditions, *J. Geophys. Res.*, *104*, 9043–9053, doi:10.1029/1998JE900018.
Daerden, F., et al. (2007), A 3D-CTM with detailed online PSC microphysics: analysis of the Antarctic winter 2003 by comparison with satellite observations, *Atmos. Chem. Phys.*, *7*, 1755–1772.
Davy, R., P. A. Taylor, W. Weng, and P.-Y. Li (2009), A model of dust in the Martian lower atmosphere, *J. Geophys. Res.*, *114*, D04108, doi:10.1029/2008JD010481.
Davy, R., J. A. Davis, P. A. Taylor, C. F. Lange, W. Weng, J. Whiteway, and H. P. Gunnlauggson (2010), Initial analysis of air temperature and related data from the Phoenix MET station and their use in estimating turbulent heat fluxes, *J. Geophys. Res.*, doi:10.1029/2009JE003444, in press.
Fuchs, N. A. (1964), *The Mechanics of Aerosols*, 408 pp., Pergamon, New York.
Gallagher, M. W., et al. (2005), An overview of the microphysical structure of cirrus clouds observed during EMERALD-1, *Q. J. R. Meteorol. Soc.*, *131*, 1143–1169, doi:10.1256/qj.03.138.
Heymsfield, A. J., D. Winker, and G.-J. van Zadelhoff (2005), Extinction-ice water content-effective radius algorithms for CALIPSO, *Geophys. Res. Lett.*, *32*, L10807, doi:10.1029/2005GL022742.

Kahn, R. A. (1990), Ice haze, snow, and the Mars water cycle, *J. Geophys. Res.*, *95*, 14,677–14,693, doi:10.1029/JB095iB09p14677.

Larsen, N. (2000), Polar stratospheric clouds. Microphysical and optical models, *Sci. Rep. 00–06*, Dan. Meteorol. Inst., Copenhagen.

Larsen, N., et al. (2002), Microphysical mesoscale simulations of polar stratospheric cloud formation constrained by in situ measurements of chemical and optical cloud properties, *J. Geophys. Res.*, *107*(D20), 8301, doi:10.1029/2001JD000999.

Larsen, N., et al. (2004), Formation of solid particles in synoptic-scale Arctic PSCs in early winter 2002/2003, *Atmos. Chem. Phys.*, *4*, 2001–2013.

Määttänen, A., H. Vehkamäki, A. Lauri, S. Merikallio, J. Kauhanen, H. Savijärvi, and M. Kulmala (2005), Nucleation studies in the Martian atmosphere, *J. Geophys. Res.*, *110*, E02002, doi:10.1029/2004JE002308.

Michelangeli, D. V., et al. (1993), Numerical simulations of the formation and evolution of water ice clouds in the Martian atmosphere, *Icarus*, *102*, 261–285, doi:10.1006/icar.1993.1048.

Mishchenko, M. I., and L. Travis (1998), Capabilities and limitations of a current Fortran implementation of the T-matrix method for randomly oriented, rotationally symmetric scatterers, *J. Quant. Spectrosc. Radiat. Transfer*, *60*, 309–324, doi:10.1016/S0022-4073(98)00008-9.

Montmessin, F., F. Forget, P. Rannou, M. Cabane, and R. M. Haberle (2004), Origin and role of water ice clouds in the Martian water cycle as inferred from a general circulation model, *J. Geophys. Res.*, *109*, E10004, doi:10.1029/2004JE002284.

Montmessin, F., P. Rannou, and M. Cabane (2002), New insights into Martian dust distribution and water-ice cloud microphysics, *J. Geophys. Res.*, *107*(E6), 5037, doi:10.1029/2001JE001520.

Murphy, J. R., O. B. Toon, R. M. Haberle, and J. B. Pollack (1990), Numerical simulations of the decay of Martian global dust storms, *J. Geophys. Res.*, *95*, 14,629–14,648, doi:10.1029/JB095iB09p14629.

Ockert-Bell, M., J. F. Bell III, J. B. Pollack, C. P. McKay, and F. Forget (1997), Absorption and scattering properties of the Martian dust in the solar wavelengths, *J. Geophys. Res.*, *102*(E4), 9039–9050, doi:10.1029/96JE03991.

Pathak, J., D. V. Michelangeli, L. Komguem, J. Whiteway, and L. K. Tamppari (2008), Simulating Martian boundary layer water ice clouds and the lidar measurements for the Phoenix mission, *J. Geophys. Res.*, *113*, E00A05, doi:10.1029/2007JE002967.

Pruppacher, H. R., and J. D. Klett (1997), *Microphysics of Clouds and Precipitation*, 2nd ed., 954 pp., Kluwer Acad., Dordrecht, Netherlands.

Richardson, M. I., R. J. Wilson, and A. V. Rodin (2002), Water ice clouds in the Martian atmosphere: General circulation model experiments with a simple cloud scheme, *J. Geophys. Res.*, *107*(E9), 5064 doi:10.1029/2001JE001804.

Tomasko, M. G., L. R. Doose, M. Lemmon, P. H. Smith, and E. Wegryn (1999), Properties of dust in the Martian atmosphere from the imager on Mars Pathfinder, *J. Geophys. Res.*, *104*, 8987–9007, doi:10.1029/1998JE900016.

Toon, O. B., R. P. Turco, J. Jordan, J. Goodman, and G. Ferry (1989), Physical processes in polar stratospheric ice clouds, *J. Geophys. Res.*, *94*, 11,359–11,380, doi:10.1029/JD094iD09p11359.

Vehkamäki, H., et al. (2007), The heterogeneous Zeldovich factor, *Atmos. Chem. Phys.*, *7*, 309–313.

Whiteway, J., M. Daly, A. Carswell, T. Duck, C. Dickinson, L. Komguem, and C. Cook (2004), Anatomy of cirrus clouds: Results from the Emerald airborne campaigns, *Geophys. Res. Lett.*, *31*, L24102, doi:10.1029/2004GL021201.

Whiteway, J., M. Daly, A. Carswell, T. Duck, C. Dickinson, L. Komguem, and C. Cook (2008), Lidar on the Phoenix mission to Mars, *J. Geophys. Res.*, *113*, E00A08, doi:10.1029/2007JE003002.

Whiteway, J., et al. (2009), Mars water ice clouds and precipitation, *Science*, *325*, 68–70.

Zent, A. P., M. H. Hecht, D. R. Cobos, S. E. Wood, T. L. Hudson, S. M. Milkovich, L. P. DeFlores, and M. Mellon (2010), Initial results from the Thermal and Electrical Conductivity Probe (TECP) on Phoenix, *J. Geophys. Res.*, doi:10.1029/2009JE003420, in press.

————————————

F. Daerden, Belgian Institute for Space Aeronomy, Ringlaan 3, B-1180 Brussels, Belgium. (frank.daerden@aeronomie.be)

R. Davy, C. Dickinson, L. Komguem, P. A. Taylor, and J. A. Whiteway, Department of Earth and Space Science and Engineering, York University, Toronto, ON M3J 1P3, Canada.

N. Larsen, Danish Meteorological Institute, DK-2100 Copenhagen, Denmark.

C. Verhoeven, Department of Mathematics, Free University of Brussels, Pleinlaan 2, B-1050 Brussels, Belgium.